

# Imaging of Long-Distance $\alpha$ -Aminoisobutyric Acid Translocation Dynamics during Resource Capture by *Serpula lacrymans*<sup>†</sup>

Monika Tlalka, Mark Fricker, and Sarah Watkinson\*

Department of Plant Sciences, University of Oxford, South Parks Road, Oxford OX1 3RB, United Kingdom

Received 7 December 2007/Accepted 3 March 2008

$\alpha$ -Aminoisobutyric acid (AIB) is a nonmetabolized amino acid analogue of alanine, which at low ( $\mu$ M) concentrations acts as a tracer for amino acid movements. At high concentrations (mM), it competitively inhibits membrane transport and metabolism of protein amino acids and acts as a systemic translocated inhibitor of mycelial extension in fungi. AIB can control mycelial spread of the basidiomycete *Serpula lacrymans*, the cause of brown rot of wood in buildings. However, it is not known how effectively the inhibitor is distributed throughout the mycelium. Realistically heterogeneous microcosms, in which the fungus grew across nutritionally inert sand to colonize discrete wood resources, were used to investigate patterns of inhibition and translocation following local application of AIB. At a 0.1 M concentration, locally applied AIB caused immediate arrest of extension throughout the whole mycelium, maintained for a 6-week experimental period. The dynamics of translocation of subtoxic amounts of [ $^{14}$ C]AIB ([ $^{14}$ C]AIB) were mapped by photon-counting scintillation imaging in conjunction with destructive harvest to establish the velocity, direction, and rate of translocation and the extent of [ $^{14}$ C]AIB reallocation accompanying the invasion of fresh wood. Locally applied [ $^{14}$ C]AIB was distributed throughout complex mycelial networks within 2 h of application, becoming localized in growing margins by 12 h. Encounter with a fresh wood resource triggered a widespread response, causing withdrawal of [ $^{14}$ C]AIB from throughout the network, accompanied by accumulation in the newly colonized wood and associated mycelium. The results are discussed in the context of nutrient dynamics in wood decomposer fungi and the mechanism of the amino acid reallocation response.

*Serpula lacrymans*, a devastating destroyer of construction timber (4, 26, 32), originated as a forest floor saprotroph (20) and diverged within the *Boletales* clade by evolving relatively recently to exploit the building environment (20). Once established from a spore infection in a wood food base (28), foraging mycelium spreads over surrounding masonry to attack further timber food sources (4). The capacity for exceptionally aggressive spread distinguishes *S. lacrymans* decay (26) from the more easily controlled decay of timber in buildings caused by its close relative *Coniophora puteana*, known as the cellar fungus.

The cord-forming mode of growth of many woodland basidiomycete fungi, including *S. lacrymans*, is seen as a developmental adaptation to a spatially heterogeneous carbon and mineral nutrient environment (3, 25, 41). Figure 1 shows the hyphal differentiation that occurs during formation of *S. lacrymans* cords.

Cords develop dynamically and responsively as nutrient channels in a transport network that supplies growing regions from spatially separate sources encountered stochastically by the foraging mycelium (11). Cords are insulated from their immediate environment by hydrophobic surfaces (30). Within them, mass flow of a variety of nutrients (16) occurs in response to changing supply and demand in different regions of

the network. While uptake is initially into cytoplasm, for long-distance mass flow in cords there must be transfers between cytoplasm and the mass flow compartment. Cords develop in *S. lacrymans* when part of the mycelium colonizes a new wood carbon source and under nitrogen limitation (40). They form behind the advancing mycelial margin as secondarily formed longitudinal aggregates of hyphae (27) centered on aseptate “vessel hyphae” (9) which are wide and relatively empty of contents. In cords imaged at various stages of development by scanning electron microscopy (15), the component hyphae become embedded in an extracellular matrix and constrained by an outer rind of fibers. There are apparently empty channels running through mature cords. The functions of these different tissues are poorly understood (5).

$\alpha$ -Aminoisobutyric acid (AIB) is a nonprotein amino acid that is taken up actively by cell membrane amino acid transporters (29), and in fungi, including *S. lacrymans*, it accumulates in the mycelial free amino acid pool (39) and is translocated through the mycelium (23, 31, 39). AIB occurs in nature as a component of peptaibol antibiotics (12) exuded by soil microfungi. It is degraded by soil bacteria (1) but has not been reported to be metabolized by eukaryotes. At concentrations of  $>0.01$  M in agar media, AIB inhibits mycelial extension in all basidiomycete species tested (8), and inhibition of *S. lacrymans* extension from wood through masonry was maintained for a 7-month experimental period (7). AIB competitively inhibits amino acid uptake and incorporation in *S. lacrymans* (39) and alters normal mycelial development by slowing or arresting the apical extension of hyphae, increasing lateral branching.

Because AIB is translocated bidirectionally in mycelial cords (39), it can affect mycelial extension at a distance from the

\* Corresponding author. Mailing address: Department of Plant Sciences, University of Oxford, South Parks Road, Oxford OX1 3RB, United Kingdom. Phone: (44) 1865 275000. Fax: (44) 1865 275074. E-mail: sarah.watkinson@plants.ox.ac.uk.

<sup>†</sup> Supplemental material for this article may be found at <http://aem.asm.org/>.

<sup>‡</sup> Published ahead of print on 14 March 2008.

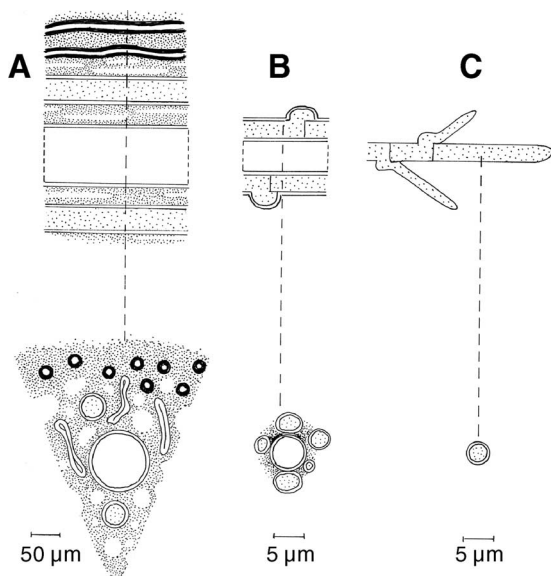


FIG. 1. Cartoon (based on references 9, 15, and 27) showing the pattern of hyphal differentiation during cord formation and the relationship between different hyphal types in mature cords. (A) Structure of mature cord. Vessel hyphae apparently empty of contents and tendril hyphae with visible cytoplasm are run longitudinally in an extracellular matrix which is permeated by longitudinal spaces. Some hyphae appear to have collapsed. Thick-walled “fiber” hyphae are run longitudinally in the outer layers of the cord. (B) A cord starting to develop approximately 50 mm behind the mycelial margin. Wider and relatively empty “vessel” hyphae become surrounded by thigmotropic “tendril” hyphae with denser cytoplasm, which grow both acropetally and basipetally over the vessel hypha surface. Extracellular matrix material binds aggregations of vessel and tendril hyphae into cords. (C) Assimilating, extending hyphal tips forming a diffuse mycelium of separate hyphae at the advancing mycelial margin. (Drawing courtesy of Rosemary Wise.)

point of uptake (7, 40). It is believed to displace protein amino acids from the mobile free amino acid pool (39), which acts both as a storage (21, 22, 37) and as a transport (6) compartment for nitrogen. It thus targets the unique adaptations of wood decay basidiomycetes to conserve nitrogen (22) in their nitrogen-limited, spatially discontinuous nutrient environment (41).

AIB acts as a systemic translocated inhibitor of mycelial growth of *S. lacrymans* from infected timber through masonry and over wood (7). It might therefore be applied for remedial treatment of decay in buildings, where local application to any accessible living mycelium might inhibit the spread of connected mycelium that is rendered inaccessible to direct treatment, for example, by being embedded in the building structure. To validate such treatment, it is necessary to establish that AIB, added at a single point, reaches the entire network.

At subtoxic concentrations ( $<10^{-5}$  M), [ $^{14}\text{C}$ ]AIB ([ $^{14}\text{C}$ ]AIB) acts as a radiolabeled tracer of amino acid translocation (2, 33, 34, 36). The novel technique of photon-counting scintillation imaging (PCSI) (2) can map the direction and velocity of movement of radiolabeled compounds at high spatial and temporal resolutions in real time (2, 33, 34). Coupled with the use of realistic microcosms to reproduce the spatial discontinuities and long time scales of the normal habitat (3, 35), PCSI with nonmetabolized nutrient analogues has been used to demon-

strate the remarkably rapid, responsive, and coordinated nutrient flow that occurs in the transport networks (11) of several cord-forming basidiomycetes during foraging growth (33, 41). This real-time imaging technique, which records dynamic changes in the two-dimensional distribution of a radioisotope, was highly appropriate to determine whether a single AIB application to one site on an exposed mycelium of *S. lacrymans* can inhibit the whole mycelium and to estimate the rate at which inhibitory amounts of AIB could be translocated to sites of growth. Furthermore, when used in conjunction with harvest to quantify [ $^{14}\text{C}$ ]AIB allocation, PCSI can determine whether colonization of fresh wood at a localized site in the mycelium induces import of amino acid.

The aims of this work were twofold: to investigate the speed and extent of AIB inhibition following application of a high concentration at a single site in the mycelial network and to test the prediction that amino acid translocation, tracked by the use of [ $^{14}\text{C}$ ]AIB at subtoxic levels, is preferentially targeted to sites of active growth and wood colonization.

## MATERIALS AND METHODS

**Culture.** *S. lacrymans* (Wulf.) ex Schroet., isolate S7 (Bundesanstalt für Materialforschung und -prüfung, Berlin, Germany), was maintained in petri dishes on malt agar (4% Oxoid malt extract, 2% Oxoid no. 3 agar) at  $22 \pm 1^\circ\text{C}$  in the dark in a temperature-controlled incubator (Gallenkamp, England).

**Experimental microcosms.** Autoclaved 1-cm<sup>3</sup> *Pinus sylvestris* sapwood blocks were colonized by *S. lacrymans* mycelium growing on malt agar for 30 to 60 days before transfer to a microcosm plate. Sand microcosm plates were 22- by 22-cm square Sterilin dishes containing 500 g of a 4:1 mixture of compacted black sand (Monro-Goundrey, United Kingdom) with acid-washed sand (VWR International Ltd., United Kingdom), evenly moistened with 80 ml deionized water. Black sand was necessary to make the white mycelium visible but was slightly hydrophobic, necessitating mixing with acid-washed sand to make a suitable growing surface for mycelium. Plates were inoculated with either one or two precolonized wood blocks and incubated in darkness at  $22^\circ\text{C}$  in polyethylene bags to maintain a high relative humidity. In some experiments, a new sterile wood block was added at a distance from the inoculated blocks to be colonized by the growing cultures during imaging.

Two microcosm arrangements were set up. The first microcosms (Fig. 2 and 3) were designed to test the effect and translocation of AIB following a single localized application at the margin of a complex network formed from the fusion of two clonal individuals grown from separate inoculum blocks. A single application, of either AIB or [ $^{14}\text{C}$ ]AIB, was made at a single point on the margin, as described below.

The second microcosm arrangement (Fig. 4) was designed to allow a mycelium preloaded with [ $^{14}\text{C}$ ]AIB as a marker to encounter and colonize one or two fresh wood blocks so that any ensuing changes in [ $^{14}\text{C}$ ]AIB distribution could be monitored. In these, [ $^{14}\text{C}$ ]AIB was applied directly to one of the inoculum blocks.

**Inhibitory AIB treatment.** In experiments for inducing inhibition, 30 µmol (given as 300 µl) of 0.1 M AIB (Sigma, United Kingdom) solution was infiltrated into a filter paper disk placed in contact with the mycelium. This allowed the relatively large volumes of AIB solution used in inhibition experiments to be maintained in contact with the hyphae while preventing percolation into the underlying sand.

**PCSI.** Imaging of [ $^{14}\text{C}$ ]AIB was done using a high-resolution photon-counting camera system (HRPCS-3; Photek Inc. St. Leonards-on-Sea, United Kingdom) as described previously (33). [ $^{14}\text{C}$ ]AIB (0.9 mM) with a specific activity of 2.11 GBq mmol<sup>-1</sup> (Amersham, United Kingdom) was used. At this concentration, [ $^{14}\text{C}$ ]AIB did not inhibit the growth of the fungus, and the specific activity was low enough not to saturate the photon signal. For PCSI, where only 9 nmol of [ $^{14}\text{C}$ ]AIB was applied to the mycelium, [ $^{14}\text{C}$ ]AIB solution was introduced as a 10-µl drop either through the filter paper disc or straight onto a mycelium-covered wood block. After being loaded with [ $^{14}\text{C}$ ]AIB, the growing colonies were covered with BioMax TranScreen LE scintillation screen (GE Healthcare, United Kingdom). The scintillation screen was laid on the mycelium in close contact with it, taking care to avoid damage. Further mycelial growth continued in the confined plane between screen and sand. Rectangular openings were cut



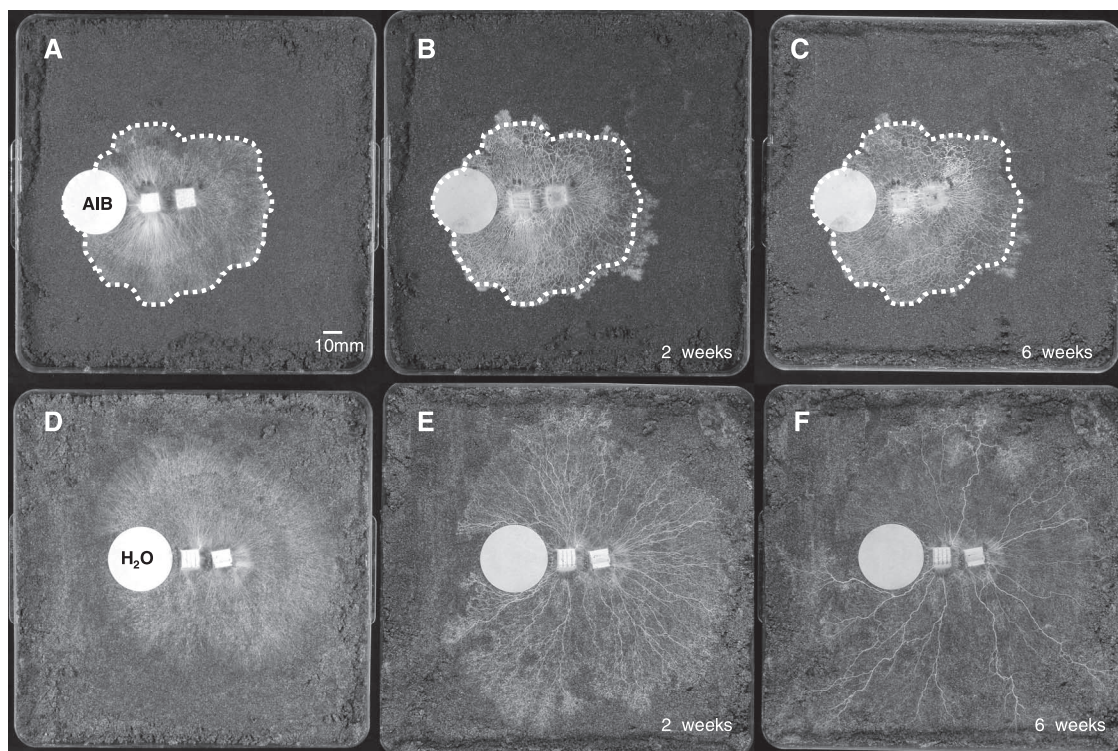


FIG. 2. Rapid and widespread inhibition of mycelial extension by 0.1 M AIB. Colonies of *Serpula lacrymans* were grown from paired adjacent precolonized wood inocula over nutrient-free moist sand in 22- by 22-cm square plastic dishes. At 10 days after inoculation, filter paper discs were placed at the mycelial margin and infiltrated with 300  $\mu$ l of either 0.1 M AIB (A to C) or deionized water (D to F). The white dotted line (A to C) indicates the position of the mycelial margin at time zero. AIB treatment induced immediate global arrest of marginal extension and a change in the pattern of development, with tightly reticulate mycelial cords in panels A to C compared with radial cords in panels D to E.

to accommodate wood blocks. Where wood block inocula were also imaged (Fig. 4), the rectangular screen cutout was placed on top of the block. The microcosms were then placed in the camera box and imaged continuously for up to 500 h with a 35-mm 1:1.4 Hama HR 0.5 $\times$  lens (Nikon, Japan).

The resulting sequence file was then analyzed using IFS32 imaging software (Photek Inc., United Kingdom), allowing for user-defined integration with images integrated over 60 min for video display and 6 or 12 h for static pictures. The signals from [ $^{14}$ C]AIB in hyphae, cords, and areas of the wood in contact with the screen were measured over time in the chosen regions. Liquid scintillation assays of [ $^{14}$ C]AIB in extracts of sand at the end of the experiment showed some leakage from the mycelium into sand, where it would be undetectable by PCSI.

The signal was calibrated to link the intensity of pixels per unit area with the molarity of [ $^{14}$ C]AIB. In brief, 10- $\mu$ l drops of [ $^{14}$ C]AIB containing the 50:50 dilutions of the compound (ranging from 1 to 18 pmol) were placed on the screen, allowed to dry, and imaged simultaneously next to the fungal microcosm under the same imaging conditions. The calibration curve showed good correlation between the molarity of [ $^{14}$ C]AIB and the intensity of the photon signal. The advantage of estimating molar quantities from image intensity was that an estimate of rate can be inferred from video imaging (e.g., Fig. 3F). However, this method gives only a minimum value, based on the signal from [ $^{14}$ C]AIB in close contact with the scintillation screen, and underestimates [ $^{14}$ C]AIB in wood and sand substrates where the increased path length of  $\beta$  emissions and photons severely attenuates the signal.

The data for the different regions were transferred into Microsoft Office Excel and were plotted against time as pmol [ $^{14}$ C]AIB mm $^{-2}$  of the selected region of the image. Changes in signal along selected cords were analyzed using Lucida 4.0 software (Kinetic Imaging, Liverpool, United Kingdom) to produce an  $x-t$  plot of intensity along the cord ( $x$ ) against time ( $t$ ). All images were assembled in Adobe Photoshop 7.0.

**Quantifying [ $^{14}$ C]AIB partitioning by liquid scintillation counting.** Quantitative fractionation following PCSI was used to measure the proportion of [ $^{14}$ C]AIB taken up that had been reallocated from the loading site into cords and fresh wood resources. After 6 weeks, different fractions of the microcosm plate

were harvested. Fractions consisted of each of either two or three wood blocks, including the original inoculum and another fresh wood block(s); the mycelial cords growing over the sand between and beyond them; and samples of the sand mycelium (microcosms 1A to C and 2A to C) (Table 1). For the sand mycelium, 10 random 1-g samples of sand were collected. Each fraction was extracted in boiling 90% ethanol and [ $^{14}$ C]AIB assayed by liquid scintillation counting of extracts. One-milliliter aliquots were pipetted directly into 4 ml OptiPhase Hisafe 3 scintillant (Fisher, United Kingdom), vortexed to mix, and counted with a Beckman LS1801  $\beta$  spectrometer (Beckman Instruments Inc.). Partitioning of [ $^{14}$ C]AIB between mycelial cords, wood blocks, and the sand mycelium (as well as the total) is given only as an estimate due to the fact that data for the whole dish were extrapolated from the 10 random sand measurements. The aim of this analysis, complementary to the PCSI imaging, was to investigate and determine the partitioning of [ $^{14}$ C]AIB between the inocula, the new wood blocks, and the remaining visible cords at the end of the experiment rather than to quantify the amount of the radiolabel in the sand. Three separate replicates were analyzed for each of the two types of microcosm described above.

## RESULTS

**Widespread fungal growth inhibition following local application of AIB.** At high concentrations, AIB solution produced a rapid and widespread effect. A single local application of 30  $\mu$ mol of AIB to the margin of a complex, fused mycelial network resulted in almost complete arrest of extension throughout the entire system, maintained throughout the 6-week experimental period (Fig. 2A to C). The more distant parts of the mycelium were equally affected, showing that inhibition was propagated irrespective of the relative positions of resources or

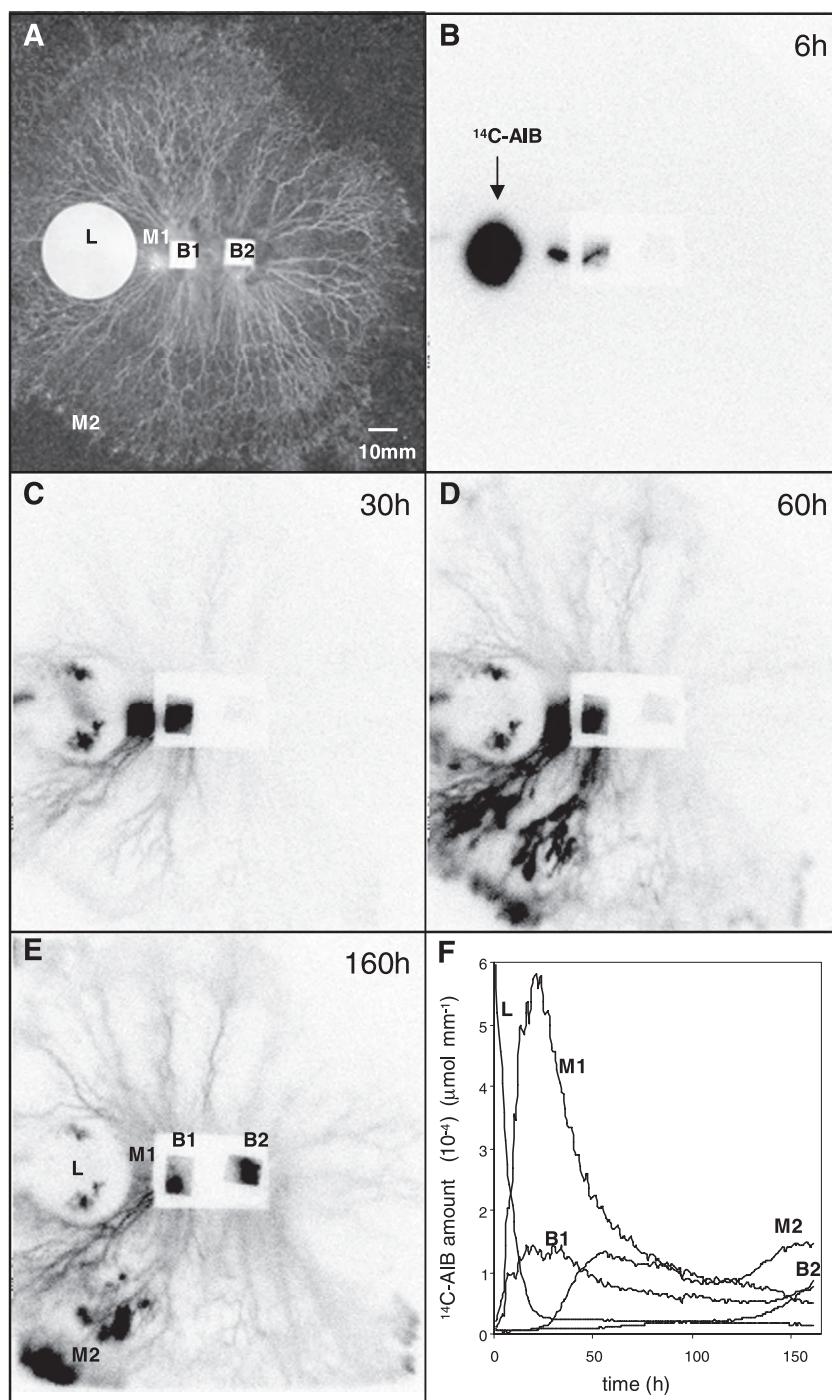


FIG. 3. [<sup>14</sup>C]AIB translocation in a complex fungal network with successive basipetal and acropetal translocation. *S. lacrymans* colonies were grown from paired adjacent inocula, and after 10 days of growth, a filter paper disc placed on the margin was infiltrated with 10 μl 0.9 mM [<sup>14</sup>C]AIB with a specific activity of 2.11 GBq mmol<sup>-1</sup> (A). The plate was covered with a scintillation screen and imaged for 160 h. Translocations and accumulation of [<sup>14</sup>C]AIB in the fungal network are shown in panels B to E. Graph F shows the time course of the photon signal over the imaging period in selected regions of interest: L, [<sup>14</sup>C]AIB loading site; M1, mycelium connecting the loading site with the proximal inoculum block; M2, a representative area of mycelium at the advancing mycelial margin; B1 and B2, wood block inocula proximal and distal, respectively, to the [<sup>14</sup>C]AIB loading site. The photon signal was integrated over 6 h. The time following loading is given in pictures; the scale bar is 10 mm.

growth sites. In controls (Fig. 2D and E), both colonies continued to extend throughout the 6-week period. Mycelial cord development was disrupted by AIB treatment, resulting in a tight reticulate network (Fig. 2C) in place of normal radial cord development (Fig. 2F).

**Spatial dynamics of locally applied [<sup>14</sup>C]AIB through a complex network.** At subtoxic concentrations, [<sup>14</sup>C]AIB did not affect mycelial extension. Following application of 9 nmol of [<sup>14</sup>C]AIB to a complex, fused mycelial network (Fig. 3A), [<sup>14</sup>C]AIB was immediately taken up from the filter paper and



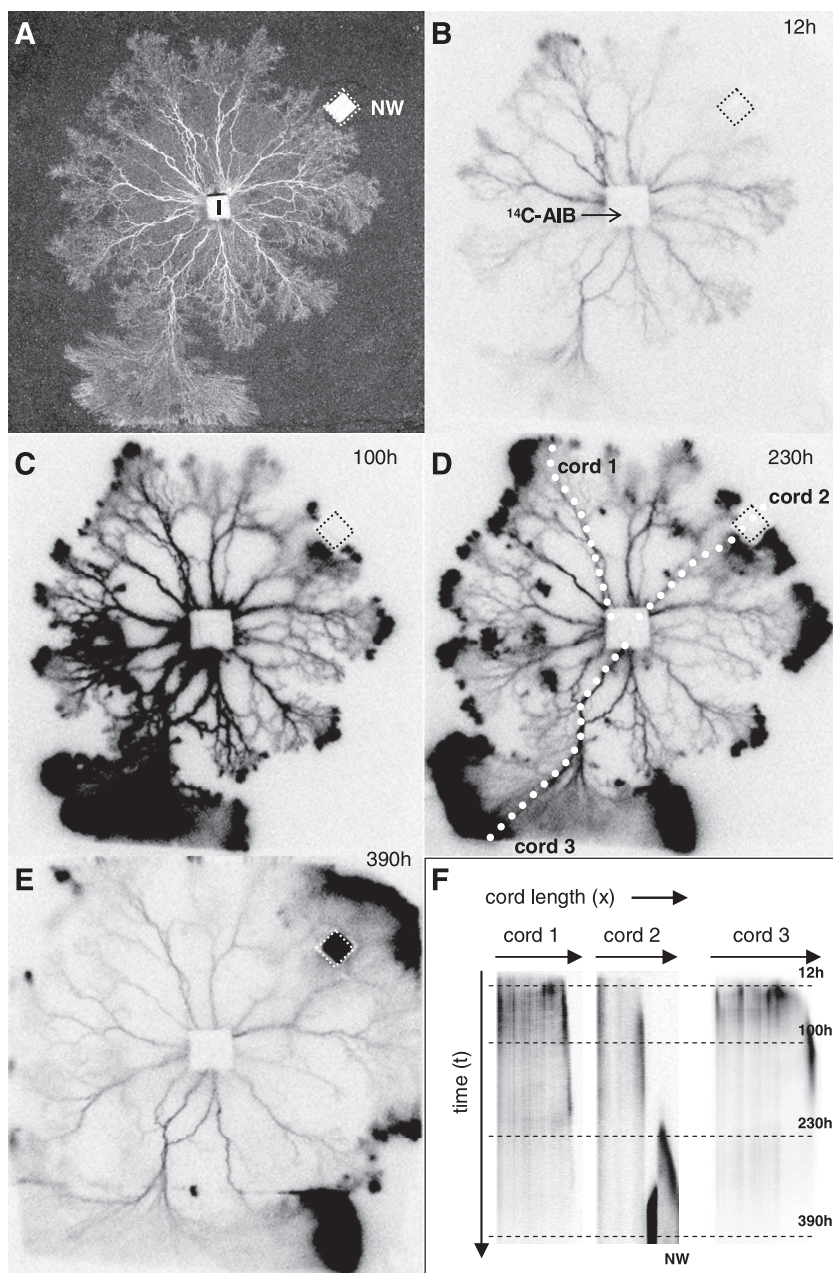
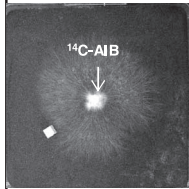
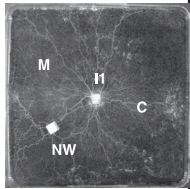
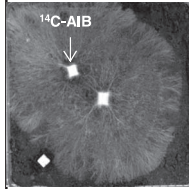
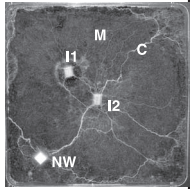


FIG. 4. Reallocation of [ $^{14}\text{C}$ ]AIB within a mycelial network induced by local colonization of a fresh wood resource. A 10-day-old mycelium grown from a colonized wood block over moist sand was loaded with  $10\ \mu\text{l}$  of  $0.9\ \text{mM}$  [ $^{14}\text{C}$ ]AIB applied directly to the top of the inoculum, and a sterile wood block (NW) was placed close to the mycelial margin (A). The whole plate, including the new wood block (but not the inoculum block, where the added [ $^{14}\text{C}$ ]AIB drop was still present), was then covered with a scintillation screen and imaged during further growth of mycelium and capture of the fresh wood resource (Fig. 3B to E). In all pictures, the photon signal was integrated over 12 h. Letters denote the inoculum loading site (I) and the new wood block (NW); time following loading is given in pictures; the scale bar is 10 mm. The relative redistribution of the label following localized resource capture is shown along the three chosen cords, indicated by dotted white lines (D). Panel F shows changes in distribution of [ $^{14}\text{C}$ ]AIB along cords 1, 2, and 3 during the imaging period. Cord 2 developed to connect the original inoculum with the fresh resource, which accumulated [ $^{14}\text{C}$ ]AIB (marked with a star), while the other two (cords 1 and 3) were not directly connected to it. In the  $x$ - $t$  diagram, generated from images B to E in Video S2 in the supplemental material, the relative intensity of the signal elicited by the presence of [ $^{14}\text{C}$ ]AIB is shown as it changed along the length of each of the three selected cords simultaneously. The cords are represented by the three parallel columns, and time is shown vertically from top to bottom, representing the 390-h recording period of Video S2 in the supplemental material. In the columns corresponding to the three selected cords, the  $x$  dimension is shown oriented outwards from the inoculum block toward the mycelial margin.

distributed throughout the system (see Video S1 in the supplemental material). Within 6 h, the signal increased in the mycelium (M1) and the first wood inoculum block (B1) (Fig. 3B). Accumulation of [ $^{14}\text{C}$ ]AIB increased in these regions in

the following 30 h (Fig. 3C and F), with some spread through the neighboring cords and a significant decrease in the loading site. By 60 h, signal had become concentrated along the margin of the entire system (Fig. 3D). By the end of recording, at

TABLE 1. Molar quantities and relative proportions of [<sup>14</sup>C]AIB in freshly colonized and partly decayed wood and mycelial cords<sup>a</sup>

Microcosm Types			<sup>14</sup> C-AIB content (pmoles)					
			Inoculum 1 (I1)	Inoculum 2 (I2)	New wood (NW)	Cords (C)	Sand mycelium <sup>e</sup> (M)	Total <sup>e</sup> (recovery in %)
		1A	50	N.A.	170	243	5594	6057 (71)
		1B*	16	N.A.	52	81	2142	2291 (27)
		1C	16	N.A.	55	97	1296	1464 (17)
		2A	41	5	222	652	2003	2923 (58)
		2B*	7	11	542	706	3717	4990 (34)
		2C	52	1145	not colonized	314	1920	3431 (40)

<sup>a</sup> Results are shown for the [<sup>14</sup>C]AIB content of inoculum wood blocks, mycelial cords, and newly colonized fresh wood blocks as well as the residue remaining in sand and in corded mycelium, estimated by scintillation counting of [<sup>14</sup>C]AIB in ethanolic extracts. Wood blocks and cords were removed and extracted separately. Total recovery (Total<sup>e</sup>) and residual [<sup>14</sup>C]AIB in uncorded mycelium and in sand plus mycelium (Sand mycelium<sup>e</sup>) were estimated from counts extracted from 10 randomized samples. Two microcosm arrangements were used, one with a single inoculum block (microcosm type 1) and the other with two separate inoculum blocks to create a more realistically complex network (microcosm type 2). Letters A, B, and C denote replicate experiments, and the data for the colonies shown are asterisked. Images show the colonies before application of [<sup>14</sup>C]AIB and at 6 weeks, immediately before harvest. In one replicate of series 2, the mycelium failed to capture the new wood block, and maximum [<sup>14</sup>C]AIB accumulated in the second block.

160 h, [<sup>14</sup>C]AIB had accumulated in the second inoculum and the associated cords and nearby margin, while signal from the first inoculum was diminished (Fig. 3E and F).

Hourly integration of the signal in the area close to the loading site showed that [<sup>14</sup>C]AIB was initially imported at a rate of at least 0.024 pmol h<sup>-1</sup> (Fig. 3F, M1). The signal from this area subsequently declined at a similar rate, coinciding with redistribution of [<sup>14</sup>C]AIB throughout the network. Measurement of different regions of the colony also showed dynamic redistribution of [<sup>14</sup>C]AIB with transient accumulations in different areas, such as the growing margins (Fig. 3F, curve M2) and the wood block inocula (compare Fig. 3D and E with curves B1 and B2 in Fig. 3F).

**AIB dynamics in response to carbon resource capture.** To test whether AIB would be preferentially redistributed from the mycelium to a newly captured wood resource, the fungus was allowed to grow on sand toward a new wood block (Fig. 4A) before being loaded with [<sup>14</sup>C]AIB through the inoculum and imaged over time (Fig. 4B to E; also see Video S2 in the supplemental material).

Within 1 to 2 h after the inoculum was loaded, [<sup>14</sup>C]AIB appeared throughout the mycelium, rapidly reaching the margin (see Video S2 in the supplemental material). Detectable signal advanced along cords with a velocity of up to 13 mm h<sup>-1</sup> (cord 3). [<sup>14</sup>C]AIB then accumulated in cords and the growing margin for up to 100 h (Fig. 4C; also see Video S2 in the supplemental material) before being slowly removed from those sites (Fig. 4D; also see Video S2 in the supplemental material). Finally, by 390 h, a strong [<sup>14</sup>C]AIB signal had appeared at the surface of the newly colonized wood (Fig. 4E; also see Video S2 in the supplemental material).

The *x-t* analysis whose results are shown in Fig. 4F is based on PCSI from Video S2 in the supplemental material and shows the dynamics of [<sup>14</sup>C]AIB within a growing mycelium (photographed in Fig. 4A) as it captured and colonized a new wood block placed in the path of mycelial advance. Three cords were selected for analysis (Fig. 4D). These cords were chosen to compare the [<sup>14</sup>C]AIB dynamics of the region of the mycelium that became connected to the fresh resource and two other regions that did not. At 12 h, the *x-t* diagram was consistent with the [<sup>14</sup>C]AIB distribution shown in Fig. 4B. The selected cords all showed detectable signals, with the lowest signal in cord 2, which later connected the inoculum and fresh wood blocks. By 100 h, [<sup>14</sup>C]AIB had accumulated at the marginal mycelium supplied by all three cords, as shown by the darkened region on the right hand side of each column, and the root of each cord at the inoculum where [<sup>14</sup>C]AIB was loaded also appears darker than the main length of each cord, perhaps reflecting continued uptake of radiolabel.

At 230 h, the marginal mycelium had reached the fresh wood block and begun to colonize it. The changes in signal pattern that occurred in the period between 230 h and 390 h indicate the redistribution of [<sup>14</sup>C]AIB that followed this colonization event. The first noticeable change was in the marginal mycelium beyond the fresh block, seen as a new, darkened region on the right of the *x-t* column representing cord 2. This area shifted toward the right with time, showing that a marginal mycelium that had accumulated large amounts of [<sup>14</sup>C]AIB continued to grow radially away from the center and, indeed, appeared to accelerate, as shown by the diagonal slope of this region of the column, not seen in any of the cords at 100 h. Comparison of Fig. 4D and E shows that the mycelium ex-

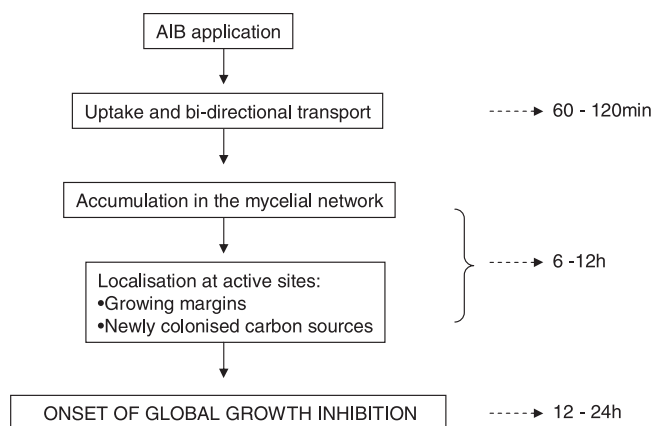


FIG. 5. AIB action in fungal microcosms. A schematic summary of the rates of uptake, accumulation in mycelium, and relocation to the mycelial margin and into a fresh wood resource based on the results is shown here.

tended several centimeters beyond the new block between 230 and 390 h.

At 390 h, there was a visible increase in signal from the new wood block itself, which started to appear at around 300 h, as seen on the  $x$ - $t$  image. This almost certainly indicates localized accumulation of [ $^{14}\text{C}$ ]AIB rather than increased biomass of [ $^{14}\text{C}$ ]AIB-labeled mycelium, because there was room for only a thin layer of mycelium between the block and the overlaid screen. By this time, [ $^{14}\text{C}$ ]AIB had almost disappeared from cords 1 and 3. Taken together with the image shown in Fig. 4E and the analysis of [ $^{14}\text{C}$ ]AIB by destructive harvest, whose results are shown in Fig. 5, this indicates that [ $^{14}\text{C}$ ]AIB was withdrawn from throughout the mycelium immediately following colonization of the fresh wood block and simultaneously imported into wood and/or mycelium at the colonization site.

To test the extent of [ $^{14}\text{C}$ ]AIB reallocation and accumulation during capture of a new carbon source, imaging by PCSI was combined with final liquid scintillation counting of microcosm fractions at the end of the 6-week experimental period. In Table 1, row 1 shows [ $^{14}\text{C}$ ]AIB partitioning in a microcosm where a wood block was added to a single colony (microcosms 1A to C) and row 2 shows a more realistic complex network resulting from fusion of adjacent mycelia (microcosms 2A to C). Table 1 gives the amount in picomoles of radiolabel recovered at the end of each experiment in each fraction for three replicate microcosms of each type.

In both types of microcosms, at harvest the freshly captured block contained significantly more [ $^{14}\text{C}$ ]AIB than the inoculum block, which had been the original site of [ $^{14}\text{C}$ ]AIB addition. Very little [ $^{14}\text{C}$ ]AIB was retained in the loaded inocula, suggesting a considerable translocation of the inhibitor to other places in the colony. This is confirmed by the presence of [ $^{14}\text{C}$ ]AIB in cords formed during the 6 weeks after loading.

In microcosm 1, the relative values of [ $^{14}\text{C}$ ]AIB distribution agreed remarkably well between replicate microcosms, with a threefold increase in fresh wood in comparison to the level in the inoculum block where [ $^{14}\text{C}$ ]AIB was applied. About 1.5 times more [ $^{14}\text{C}$ ]AIB was retained in the corded mycelium overlying the sand than in the new wood.

In the more complex network of microcosm 2, again [ $^{14}\text{C}$ ]AIB was preferentially allocated to the fresh wood block after transient accumulation in the first one (Table 1, row 2). In one microcosm (Fig. 3B), the advancing mycelium grew past the fresh block and did not colonize it. Here, most of the [ $^{14}\text{C}$ ]AIB held within cords and wood was allocated to the second block, which thus appeared to act as a transfer point from which [ $^{14}\text{C}$ ]AIB would probably be exported if a further resource were colonized. In both microcosm types, significant amounts of [ $^{14}\text{C}$ ]AIB were contained in the visible cords. The rest remained in the surrounding sand. It was not possible to separate uncorded diffuse mycelium from sand particles for analysis by scintillation counting. The [ $^{14}\text{C}$ ]AIB estimated to remain in the sand-plus-mycelium fraction includes that concentrated in the mycelial margins, as shown in Fig. 4, and any [ $^{14}\text{C}$ ]AIB released by the mycelial autolysis that accompanies remodeling of initial growth into the corded network (40).

The schematic diagram in Fig. 5 summarizes the results of the experiments described above to show the dynamics of AIB following uptake. Widespread translocation followed within 1 to 2 h, with selective distribution to mycelial margins and new resources through cords initiated by 12 h, accompanied by arrest of further extension, which was maintained throughout an experimental period of 6 weeks.

## DISCUSSION

Locally applied 0.1 M AIB exerted a durable inhibitory effect throughout the entire complex network of *Serpula lacrymans*. Growth was evenly arrested round the entire margin, indicating that locally applied AIB was rapidly distributed from the application site throughout the network, irrespective of the relative positions of food sources and growing regions. PCSI in parallel systems revealed the underlying dynamics of [ $^{14}\text{C}$ ]AIB translocation. The pattern was similar to those previously seen in other cord-forming fungi. Bidirectional transport, both toward and away from the original direction of growth, occurred in mycelial networks of *Phanerochaete velutina* formed when mycelium from a single inoculum had colonized a number of separate cellulose filter paper resources and formed cords between them (36). Simultaneous bidirectional translocation in cords of *Hypholoma fasciculare* was demonstrated by double labeling with  $^{32}\text{P}$  and  $^{33}\text{P}$  loaded at opposite ends of a corded mycelium (24).

A system-wide coordinated sequence of changes was involved in the reallocation response triggered by capture of a fresh wood block, with import of amino acid occurring about 100 h after the mycelium of *S. lacrymans* first contacted the new resource. AIB was imported into the fresh wood resource by a global coordinated response of the network following initial colonization. Furthermore, in the more complex system translocation was revealed by PCSI to be highly dynamic, continuously distributing and reallocating AIB during the tracking period. The relative amounts of [ $^{14}\text{C}$ ]AIB in the cords at the end of the imaging period (Fig. 4F) show almost complete withdrawal of [ $^{14}\text{C}$ ]AIB from mycelium distal to the new resource.

Scintillation counting of [ $^{14}\text{C}$ ]AIB in separate microcosm fractions at the end of the imaging period indicated preferential import of [ $^{14}\text{C}$ ]AIB into the fresh resource. This was con-



sistent with PCSI results and in addition confirmed that AIB import was not simply the result of an increase in the amount of AIB-loaded mycelium resulting from growth but that translocated AIB had accumulated in fresh wood and in cords connected to it, at the expense of distant mycelium.

The results demonstrate for the first time that a mycelial network of a wood decay fungus responds to freshly colonized wood by importing a significant proportion of its total nitrogen resources. In ecosystems, import of nitrogen by saprotrophic decomposer fungi in the decomposer subsystem of the upper soil horizons can facilitate decomposition of nitrogen-poor lignocellulosic plant remains (10). Fungal N translocation can increase cellulolysis that is otherwise N limited (38). The mycelium of woodland fungi can hold ecologically significant proportions of available soil nitrogen (41), and the extent to which this is imported into lignocellulosic plant remains on the soil surface may influence ecosystem carbon budgets. Cord-forming wood decay fungi may thus act as a link between carbon release and nitrogen dynamics in ecosystems (25, 35, 41). The high proportion of free amino acid retained within the mycelial cords (Table 1) is consistent with previous work (22) which showed that basidiomycetes accumulate amino acids from the environment in excess of immediate metabolic requirements and store them in the expandable free amino pool and in protein (37).

AIB is believed to follow the same translocation path as protein amino acids, because it is accumulated in the free amino acid pool and moves at rates comparable with those of other radiolabeled nutrients (16). The physiological mechanism of the translocation stream of fungi is poorly understood (5) but appears to transport a wide range of nutrients and water by mass flow (14, 16, 33). Imaging experiments with [ $^{14}\text{C}$ ]glutamic acid as described previously (M. Tlalka, M. D. Fricker, and S. C. Watkinson, presented at the 38th Symposium of the International Research Group on Wood Preservation, Jackson, WY, 20 to 24 May 2007) indicate that AIB follows the same path through cords, although unlike glutamate, it is not removed from the translocation stream by metabolism and incorporation. Its inhibitory effects therefore are likely to increase with time, as the intracellular concentration rises relative to the level of utilizable amino acid.

The mechanism of the amino acid reallocation response to a fresh carbon source is not known. A similar dynamic reallocation of phosphorus occurred in foraging mycelium of the forest floor wood decomposer *Phanerochaete velutina*, where phosphate labeled with  $^{32}\text{P}$  was preferentially translocated within the cord system into the least-decayed, largest carbon resource out of several that the mycelium had colonized (13, 42). The authors suggested that the network of cords carries a bidirectional translocation stream of nutrients, which are locally unloaded in response to local demand at sites of enhanced metabolism or growth. The results presented here are consistent with this interpretation. Hyphae in new wood blocks and at the mycelial margins represent the most metabolically active sites in the network, where nutrients are probably actively withdrawn into cytoplasm from the mass flow channel. The amounts of accumulation of AIB over long periods, as shown in Fig. 4, do not reflect the pattern of localization of protein amino acids such as glutamate, because these are rapidly me-

tabolized. However, the results illuminate the mechanism of amino acid translocation in fungal networks.

Accumulation of AIB at metabolically active sites suggests the local induction of an active amino acid transport process removing amino acid from the mass flow translocation stream in cords. A plasma membrane boundary or boundaries between cytoplasm and the mass flow pathway in cords have been inferred (5, 34), but the cellular anatomy and position of the boundary between cytoplasmic and mass flow are still obscure (5).

AIB as an inhibitor of mycelial extension thus appears to target the amino acid translocation that is a fundamental physiological adaptation in basidiomycete wood decay fungi. The results validate the use of AIB as a translocated systemic inhibitor of mycelial extension for controlling dry rot. Because it is rapidly translocated to sites of attack, where it stops further mycelial advance, AIB treatment is considered to be a suitable first step in controlling basidiomycete decay in buildings to limit spread through inaccessible parts of a building. It potentially acts as a "magic bullet," because it usurps the normal physiology of the fungus to reach hidden sites of growth and attack. In large buildings with endemic dry rot, embedded mycelia originating from separate spore infections probably fuse into extensive networks because of the widespread vegetative compatibility in *S. lacrymans* (17–19). Our results show that AIB is rapidly translocated throughout complex, fused networks from a localized point of application. Inhibition of spread through masonry persists for months following application to infected wood (7). These results justify further investigation using extensive mycelium in buildings to establish the extent and durability of locally applied AIB inhibition of *S. lacrymans*. In historic conservation, AIB could prevent infection of valuable timber and cellulose materials in the vicinity of an outbreak, holding the spread of dry rot until the underlying damp conditions can be cured and reducing the need for destructive eradication treatment (4).

#### ACKNOWLEDGMENTS

This work was supported by grants UK NERC GR3/12946, UK NERC/A/S/2002/882, and UK BBSRC 43/P19284.

The culture of *S. lacrymans* isolate S7 was kindly supplied by Olaf Schmidt, University of Hamburg. We are grateful for photography by John Baker and technical assistance from Caroline O'Brien.

#### REFERENCES

1. Aaslestad, H. G., and A. D. Larson. 1964. Bacterial metabolism of 2-methylalanine. *J. Bacteriol.* **88**:1296–1303.
2. Bebb, D. P., M. Tlalka, J. Hynes, P. R. Darrah, A. E. Ashford, S. C. Watkinson, L. Boddy, and M. D. Fricker. 2006. Imaging complex nutrient dynamics in mycelial networks, p. 3–21. In G. M. Gadd, S. C. Watkinson, and P. S. Dyer (ed.), *Fungi in the environment*. Cambridge University Press, Cambridge, United Kingdom.
3. Boddy, L. 1999. Saprotrophic cord-forming fungi: meeting the challenge of heterogeneous environments. *Mycologia* **91**:13–32.
4. Bravery, A. F. 1991. The strategy for the eradication of *Serpula lacrymans*, p. 117–130. In D. H. Jennings and A. F. Bravery (ed.), *Serpula lacrymans: fundamental biology and control strategies*. Wiley, Chichester, United Kingdom.
5. Cairney, J. W. G. 1992. Translocation of solutes in ectomycorrhizal and saprotrophic rhizomorphs. *Mycol. Res.* **96**:135–141.
6. Darrah, P. R., M. Tlalka, A. E. Ashford, S. C. Watkinson, and M. D. Fricker. 2006. The vacuole system is a significant intracellular pathway for longitudinal solute transport in basidiomycete fungi. *Eukaryot. Cell* **5**:1111–1125.
7. Dobson, J., J. Power, J. Singh, and S. C. Watkinson. 1993. The effectiveness of 2-aminoisobutyric acid as a translocatable fungistatic agent for the remedial treatment of dry rot caused by *Serpula lacrymans* in buildings. *Int. Biodeterior. Biodegrad.* **31**:129–141.



8. Elliot, M. L., and S. C. Watkinson. 1989. The effect of  $\alpha$ -aminoisobutyric acid on wood decay and wood spoilage fungi. *Int. Biodeterior.* **25**:355–371.
9. Falck, R. 1912. Die Meruliusfaule des Bauholzes, p. 1–405. In A. Moeller (ed.), *Hauschwammforschungen* 6. Gustav Fischer, Jena, Germany.
10. Frey, S. D., E. T. Elliott, K. Paustian, and G. Peterson. 2000. Fungal translocation as a mechanism of exogenous nitrogen inputs to decomposing surface residues in a no-tillage agroecosystem. *Soil Biol. Biochem.* **32**:689–698.
11. Fricker, M. D., L. Boddy, and D. P. Bebber. 2007. Network organisation of mycelial fungi, p. 309–330. In R. J. Howard and N. A. R. Gow (ed.), *Biology of the fungal cell*, 2nd ed. The mycota, vol. 8. Springer-Verlag, Berlin, Germany.
12. Hoffmeister, D., and N. P. Keller. 2007. Natural products of filamentous fungi. *Nat. Prod. Rep.* **24**:393–416.
13. Hughes, C. L., and L. Boddy. 1996. Sequential encounter of wood resources by mycelial cords of *Phanerochaete velutina*: effect on growth patterns and phosphorus allocation. *New Phytol.* **133**:713–726.
14. Jennings, D. H. 1994. Translocation in mycelia, p. 163–173. In J. G. H. Wessels and H. Meinhardt (ed.), *The mycota. I. Growth, differentiation and sexuality*. Springer-Verlag, Berlin, Germany.
15. Jennings, L., and S. C. Watkinson. 1982. The structure and development of mycelial strands in *Serpula lacrymans*. *Trans. Br. Mycol. Soc.* **78**:465–474.
16. Jentschke, G., B. Brandes, A. J. Kuhn, W. H. Schroder, and D. L. Godbold. 2001. Interdependence of phosphorus, nitrogen, potassium and magnesium translocation by the ectomycorrhizal fungus *Paxillus involutus*. *New Phytol.* **149**:327–337.
17. Kausrud, H., O. Schmidt, M. Elfstrand, and N. Högborg. 2004. Extremely low AFLP variation in the European dry rot fungus (*Serpula lacrymans*): implications for self/nonself-recognition. *Mycol. Res.* **108**:1264–1270.
18. Kausrud, H. 2004. Widespread vegetative compatibility groups in the dry rot fungus *Serpula lacrymans*. *Mycologia* **96**:232–239.
19. Kausrud, H., G.-P. Sætre, O. Schmidt, C. Decock, and T. Schumacher. 2006. Genetics of self/nonself recognition in *Serpula lacrymans*. *Fungal Genet. Biol.* **43**:503–510.
20. Kausrud, H., I. B. Svegård, G.-P. Sætre, H. Knudsen, Ø. Stensrud, O. Schmidt, S. Doi, T. Sugiyama, and N. Högborg. 2007. Asian origin and rapid global spread of the destructive dry rot fungus *Serpula lacrymans*. *Mol. Ecol.* **16**:3350–3360.
21. Klionsky, D. J., P. K. Herman, and S. D. Emr. 1990. The fungal vacuole: composition, function and biogenesis. *Microbiol. Rev.* **54**:266–292.
22. Levi, M. P., and E. B. Cowling. 1969. Role of nitrogen in wood deterioration. VII. Physiological adaptation of wood destroying fungi and other fungi to substrates deficient in nitrogen. *Phytopathology* **59**:460–468.
23. Lilly, W. W., S. M. Higgins, and G. J. Wallweber. 1990. Uptake and translocation of 2-aminoisobutyric acid by *Schizophyllum commune*. *Exp. Mycol.* **14**:169–177.
24. Lindahl, B., R. Finlay, and S. Olsson. 2001. Simultaneous, bidirectional translocation of  $^{32}$ P and  $^{33}$ P between wood blocks connected by mycelial cords of *Hypholoma fasciculare*. *New Phytol.* **150**:189–194.
25. Lindahl, B. O., A. F. S. Taylor, and R. D. Finlay. 2002. Defining nutritional constraints on carbon cycling in boreal forests—towards a less 'phytogenic' perspective. *Plant Soil* **242**:123–135.
26. Money, N. P. 2006. Plagues upon houses and cars: the unnatural history of *Meruliporia incrassata*, *Serpula lacrymans* and *Sphaerobolus stellatus*, p. 289–309. In G. M. Gadd, S. C. Watkinson, and P. S. Dyer (ed.), *Fungi in the environment*. Cambridge University Press, Cambridge, United Kingdom.
27. Moore, D. H. 1998. *Fungal morphogenesis*. Cambridge University Press, Cambridge, United Kingdom.
28. Nuss, I., D. H. Jennings, and C. J. Veltkamp. 1991. Morphology of *Serpula lacrymans*, p. 9–38. In D. H. Jennings and A. F. Bravery (ed.), *Serpula lacrymans: fundamental biology and control strategies*. Wiley, Chichester, United Kingdom.
29. Ogilvie-Villa, S., R. M. DeBusk, and A. G. DeBusk. 1981. Characterization of 2-aminoisobutyric acid transport in *Neurospora crassa*: a general amino acid permease-specific substrate. *J. Bacteriol.* **147**:944–948.
30. Olsson, P. A., I. Jakobsen, and H. Wallander. 2002. Foraging and resource allocation strategies of mycorrhizal fungi in a patch environment, p. 93–115. In M. G. A. van der Heijden and I. Sanders (ed.), *Mycorrhizal ecology, ecological studies*, vol. 157. Springer, Berlin, Germany.
31. Olsson, S., and S. N. Gray. 1998. Patterns and dynamics of  $^{32}$ P phosphate and  $^{14}$ C labeled AIB translocation in intact basidiomycete mycelia. *FEMS Microbiol. Ecol.* **26**:109–120.
32. Ramsbottom, J. 1953. *Mushrooms and toadstools: a study of the activities of fungi*, p. 233–246. Collins, London, United Kingdom.
33. Tlalka, M., S. C. Watkinson, P. R. Darrah, and M. D. Fricker. 2002. Continuous imaging of amino-acid translocation in intact mycelia of *Phanerochaete velutina* reveals rapid, pulsatile fluxes. *New Phytol.* **153**:173–184.
34. Tlalka, M., D. Hensman, P. R. Darrah, S. C. Watkinson, and M. D. Fricker. 2003. Non-circadian oscillations in amino-acid transport have complementary profiles in assimilatory and foraging hyphae of *Phanerochaete velutina*. *New Phytol.* **158**:325–335.
35. Tlalka, M., D. P. Bebber, P. R. Darrah, and S. C. Watkinson. 2007. Mycelial networks: nutrient uptake, translocation, and role in ecosystems, p. 43–62. In L. Boddy, J. C. Frankland, and P. van West (ed.), *Ecology of saprotrophic basidiomycetes*. Elsevier, Oxford, United Kingdom.
36. Tlalka, M., D. P. Bebber, P. R. Darrah, S. C. Watkinson, and M. D. Fricker. 2007. Emergence of self-organised oscillatory domains in fungal mycelia. *Fungal Genet. Biol.* **44**:1085–1095.
37. Venables, C. E., and S. C. Watkinson. 1989. Medium induced changes in patterns of free and combined amino acids in mycelium of *Serpula lacrymans*. *Mycol. Res.* **3**:273–277.
38. Watkinson, S. C., E. M. Davison, and J. Bramah. 1981. The effect of nitrogen availability on growth and cellulolysis by *Serpula lacrymans*. *New Phytol.* **89**:295–305.
39. Watkinson, S. C. 1984. Inhibition of growth and development of *Serpula lacrymans* by the non-metabolised amino acid analogue 2-aminoisobutyric acid. *FEMS Microbiol. Lett.* **24**:247–250.
40. Watkinson, S. C. 1999. Metabolism and hyphal differentiation in large basidiomycete colonies, p. 126–156. In N. A. R. Gow, G. D. Robson, and G. M. Gadd (ed.), *The fungal colony*. Cambridge University Press, Cambridge, United Kingdom.
41. Watkinson, S. C., D. P. Bebber, P. R. Darrah, M. D. Fricker, M. Tlalka, and L. Boddy. 2006. The role of wood decay fungi in the carbon and nitrogen dynamics of the forest floor, p. 149–181. In G. M. Gadd (ed.), *Fungi in biogeochemical cycles*. Cambridge University Press, Cambridge, United Kingdom.
42. Wells, J. M., J. M. Harris, and L. Boddy. 1998. Temporary phosphorus partitioning in mycelial systems of the cord-forming basidiomycete *Phanerochaete velutina*. *New Phytol.* **140**:283–293.